Computational Mechanistic Studies on Enantioselective pybox−Ruthenium-Catalyzed Cyclopropanation Reactions

Alfonso Cornejo,[†] José M. Fraile,[‡] José I. García,*[,‡] María J. Gil,[†] Víctor Martínez-Merino,*[,†] José A. Mayoral,[‡] and Luis Salvatella[‡]

Departamento de Química Orgánica, Instituto de Ciencia de Materiales de Aragón, CSIC-Universidad de Zaragoza, Instituto Universitario de Catálisis Homogénea, Universidad de Zaragoza, Pedro Cerbuna 12, E-50009 Zaragoza, Spain, and Departamento de Química Aplicada, Universidad Pública de Navarra, E-31006 Pamplona, Spain

Received April 18, 2005

The mechanism of the ruthenium(II)-catalyzed cyclopropanation reaction of olefins with diazo compounds has been extensively investigated for a medium-sized reaction model by means of DFT calculations. The starting ethylene complex of the dichloro[(*E*)-2-(methylimino)-*N*-(1*E*,2*E*)-2-(methyliminoethylidene)ethanamine]ruthenium(II) catalyst undergoes a ligand exchange with methyl diazoacetate to yield a reaction intermediate, which subsequently undergoes nitrogen extrusion to generate a ruthenium−carbene complex. The cyclopropanation step takes place through a direct carbene addition of the ruthenium carbene species to the olefin double bond to yield a catalyst-product complex, which can finally regenerate the starting complex. Stereochemical considerations on a "real-world" system—the cyclopropanation reaction of styrene with methyl diazoacetate, catalyzed by a chiral pybox−ruthenium complex—have been investigated by means of full quantum-mechanical calculations on this reaction. The theoretical results show excellent agreement with the experimental observations and allow a mechanistic explanation to be advanced concerning the origin of the stereoselectivities observed. The explanation is based on the intermolecular steric interaction between the alkene and one of the isopropyl groups of the chiral ligand in the disfavored approaches. The model developed also provides an explanation for some particular stereoelectronic behavior of pybox ligands, such as the remote stereoelectronic effects and the good enantioselectivities described with C_1-pybox ligands.

Introduction

Cyclopropane derivatives are an important family of chemical compounds due to their interesting biological properties[1] as well as their use as starting materials and intermediates in organic synthesis.[2] As a result, great efforts have been made to develop efficient diastereo- and enantioselective methods for the synthesis of cyclopropanes.[3,4] A particularly versatile method is the metal-catalyzed cyclopropanation of olefins with diazo compounds, for which various efficient homogeneous catalysts have been developed.

Highly effective and stereocontrolled cyclopropanation reactions involving transition-metal-catalyzed decomposition of diazoalkanes have been achieved with metal complexes of copper[5] and rhodium[6] and, to a lesser extent, complexes of other transition metals such as cobalt.[4,7]

Only in recent years have ruthenium complexes been described as efficient catalysts for these kinds of reactions.[8] The asymmetric version of these processes can be efficiently carried out using chiral 2,6-bis(oxazolin-2-yl)pyridine (pybox) ligands.[4,8,9] Different structural variations on the pybox structure have been studied in

* To whom correspondence should be addressed. J.I.G.: e-mail, jig@unizar.es; tel, +34 976762271; fax, +34 976762077. V.M.-M.: e-mail, merino@unavarra.es; tel, +34 948169595; fax, +34 948169606.

[†] Universidad Pública de Navarra.

[‡] Universidad de Zaragoza.

(1) Suckling, C. J. *Angew. Chem., Int. Ed. Engl.* **1988**, *27*, 537−552.

(2) Wong, H. N. C.; Hon, M.-Y.; Tse, C.-W.; Yip, Y.-C.; Tanko, J.; Hudlicky, T. *Chem. Rev.* **1989**, *89*, 165−198.

(3) (a) Ye, T.; McKervey, M. A. *Chem. Rev.* **1994**, *94*, 1091−1160. (b) Singh, V. K.; Gupta, A. D.; Sekar, G. *Synthesis* **1997**, 137−149. (c) Doyle, M. P.; Protopopova, M. N. *Tetrahedron* **1998**, *54*, 7919−7946. (d) Lebel, H.; Marcoux, J.-F.; Molinaro, C.; Charette, A. B. *Chem. Rev.* **2003**, *103*, 977−1050.

(4) Lebel, H.; Marcoux, J.-F.; Molinaro, C.; Charette, A. B. *Chem. Rev.* **2003**, *103*, 977−1050 and references therein.

(5) Pfaltz, A. Cyclopropanation and C−H Insertion with Cu. In *Comprehensive Asymmetric Catalysis*; Jacobsen, E. N., Pfaltz, A., Yamamoto, H., Eds.; Springer-Verlag: Berlin, 1999; Vol. 2, pp 513−538.

(6) Lydon, K. M.; McKervey, M. A. Cyclopropanation and C−H Insertion with Rh. In *Comprehensive Asymmetric Catalysis*; Jacobsen, E. N., Pfaltz, A., Yamamoto, H., Eds.; Springer-Verlag: Berlin, 1999; Vol. 2, pp 539−580.

(7) For recent examples see: (a) Ikeno, T.; Iwakura, I.; Yabushita, S.; Yamada, T. *Org. Lett.* **2002**, *4*, 517−520. (b) Ikeno, T.; Iwakura, I.; Yamada, T. *J. Am. Chem. Soc.* **2002**, *124*, 15152−15153. (c) Ikeno, T.; Iwakura, I.; Yamada, T. *Org. Lett.* **2004**, *6*, 949−952.

(8) (a) Charette, A. B.; Lebel, H. Cyclopropanation and C−H Insertion with Metals other than Cu and Rh. In *Comprehensive Asymmetric Catalysis*; Jacobsen, E. N., Pfaltz, A., Yamamoto, H., Eds.; Springer-Verlag: Berlin, 1999; Vol. 2, pp 581−603. (b) Maas, G. *Chem. Soc. Rev.* **2004**, *33*, 183−190. (c) Nishiyama, H. *Top. Organomet. Chem.* **2004**, *11*, 81−92. (d) Nishiyama, H. In *Advances in Catalytic Processes*; Doyle, E. P., Ed.; JAI Press: London, 1997; Vol. 2 (Asymmetric Catalysis), pp 153−188.

(9) Desimoni, G.; Faita, G.; Quadrelli, P. *Chem. Rev.* **2003**, *103*, 3119−3154 and references therein.

10.1021/om050300v CCC: $30.25
Publication on Web 06/04/2005

Scheme 1. Possible Catalytic Cycles for Ruthenium-Catalyzed Cyclopropanation Reactions

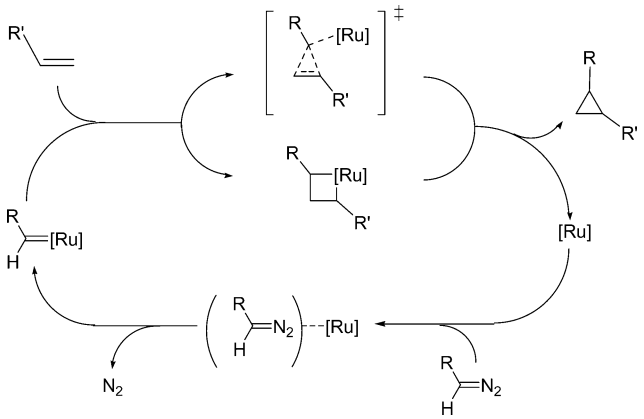

an effort to improve the enantioselectivities, and some unexpected results have been observed: e.g., the electronic effect of substituents in the 4-position of the pyridine ring on the enantioselectivity[10] and the good enantioselectivities obtained with C_1-symmetric pybox ligands.[11]

From the point of view of large-scale applications, the ease of use and recovery of chiral catalysts have become important and our group has pioneered the immobilization of this kind of catalytic system.[12]

It is generally accepted that the mechanism of the transition-metal-catalyzed cyclopropanation reaction involves a metal−carbene complex, which is formed by association of the diazo compound and the catalyst with concomitant extrusion of nitrogen. Unlike copper and rhodium carbenes, which are much more elusive, a number of ruthenium carbene complexes have been either isolated[13] or detected spectroscopically.[14] These complexes transfer their carbene ligand to styrene and are able to catalyze the cyclopropanation of alkenes with diazooacetates.[13b,c]

Two different mechanisms can be proposed for the carbene transfer from the ruthenium carbene complex to an alkene (Scheme 1), and these are the concerted pathway (henceforth referred to as direct carbene addition) and a two-step process that involves a ruthenacyclobutane intermediate. Ruthenium carbenes that do not have an additional vacant coordination site at the metal, such as the pybox−$RuCl_2$−carbene complexes, are expected to react by the concerted pathway, which also prevails for rhodium- and copper-catalyzed reactions.[15]

However, despite the increasing interest in chiral pybox−ruthenium catalysts for enantioselective cyclopropanation reactions, theoretical studies of the catalytic cycle and the operating stereodifferentiation mechanisms have yet to be published. An asymmetric induction model, based on DFT calculations of a chiral Schiff base ruthenium carbene intermediate structure, has recently been reported.[16] On the other hand, theoretical studies on the closely related ruthenium-catalyzed cross-metathesis reaction have been published very recently,[17] including a small reference to possible concurrent cyclopropanation pathways[17a] and to the asymmetric reaction with chiral catalysts.[17c]

Scheme 2. Nonchiral Model Ru-Catalyzed Cyclopropanation Reaction

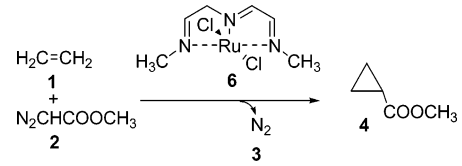

In this paper we present a thorough study of the mechanism of the pybox−ruthenium(II)-catalyzed cyclopropanation reactions by means of a theoretical approach based on density functional theory (DFT) calculations. The catalytic cycle has been studied on a simplified nonchiral model (see Models and Computational Details). Particular attention has been paid to the stereoselectivity-determining step of the catalytic cycle, which has been studied on a "real world" model: i.e., the reaction of methyl diazoacetate with styrene catalyzed by the dichloro(2,6-bis[(*S*)-4-isopropyloxazolin-2-yl]pyridine)ruthenium(II) complex (henceforth (^{i}Pr)pybox-$RuCl_2$).

Models and Computational Details

A comprehensive mechanistic study of the ruthenium-catalyzed cyclopropanation reaction was carried out by means of a medium-sized model that included a number of simple reactants: dichloro[(*E*)-2-(methylimino)-*N*-(1*E*,2*E*)-2-(methyliminoethylidene)ethanamine]ruthenium(II) (**6**) as the catalyst, ethylene (**1**) as the olefin, and methyl diazoacetate (**2**) as the diazo compound (Scheme 2). The formation of the ruthenium carbene complex and the possible pathways for the cyclopropanation reaction were studied with this model.

It should be noted that the ligand (*E*)-2-(methylimino)-*N*-(1*E*,2*E*)-2-(methyliminoethylidene)ethanamine (henceforth triimine) does not possess C_2 symmetry, unlike most of the real pybox ligands. The question of the suitability of this triimine as a good model for the real ligand is pertinent, and for this reason, particular attention was paid to this point (see below).

The possibility of different conformations was taken into account where appropriate, although the discussion of the results is centered on the most stable form in each case.

(10) Park, S.-B.; Murata, K.; Matsumoto, H.; Nishiyama, H. *Tetrahedron: Asymmetry* **1995**, *6*, 2487−2494.

(11) Nishiyama, H.; Soeda, N.; Naito, T.; Motoyama, Y. *Tetrahedron: Asymmetry* **1998**, *9*, 2865−2869.

(12) (a) Cornejo, A.; Fraile, J. M.; García, J. I.; Gil, M. J.; Legarreta, G.; Luis, S. V.; Martínez-Merino, V.; Mayoral, J. A. *Org. Lett.* **2002**, *4*, 3927−3930. (b) Cornejo, A.; Fraile, J. M.; García, J. I.; Gil, M. J.; Martínez-Merino, V.; Mayoral, J. A. *Mol. Diversity* **2003**, 93−105.

(13) (a) Park, S.-B.; Nishiyama, H.; Itoh, Y.; Itoh, K. *J. Chem. Soc., Chem. Commun.* **1994**, 1315−1316. (b) Park, S.-B.; Sakata, N.; Nishiyama, H. *Chem. Eur. J.* **1996**, *2*, 303−306. (c) Che, C.-M.; Huang, J. S.; Lee, F.-W.; Li, Y.; Lai, T.-S.; Kwong, H.-L.; Teng, P.-F.; Lee, W.-S.; Lo, W.-C.; Peng, S. M.; Zhou, Z.-Y. *J. Am. Chem. Soc.* **2001**, *123*, 4119−4129.

(14) (a) Galardon, E.; Le Maux, P.; Simmoneaux, G. *Chem. Commun.* **1997**, 927−928. (b) Lee, H. M.; Bianchini, C.; Jia, G.; Barbaro, P. *Organometallics* **1999**, *18*, 1961−1966. Bianchini, C.; Lee, H. M. *Organometallics* **2000**, *19*, 1833−1840.

(15) For recent theoretical studies on copper- and rhodium-catalyzed cyclopropanation reactions, see: (a) Fraile, J. M.; García, J. I.; Martínez-Merino, V.; Mayoral, J. A.; Salvatella, L. *J. Am. Chem. Soc.* **2001**, *123*, 7616−7625. (b) Rasmussen, T.; Jensen, J. F.; Østergaard, N.; Tanner, D.;.Ziegler, T.; Norrby, P.-O. *Chem. Eur. J.* **2002**, *8*, 177−184. (c) Straub, B. F.; Gruber, I.; Rominger, F.; Hofmann, P. *J. Organomet. Chem.* **2003**, *684*, 124−143. (d) Suenobu, K.; Itagaki, M.; Nakamura, E. *J. Am. Chem. Soc.* **2004**, *126*, 7271−7280. (e) Nowlan, D. T.; Gregg, T. M.; Daves, H. M. L.; Singleton, D. A. *J. Am. Chem. Soc.* **2003**, *125*, 15902−15911.

(16) Munslow, I. J.; Gillespie, K. M.; Deeth, R. J.; Scott, P. *Chem. Commun.* **2001**, 1638−1639.

(17) (a) Bernardi, F.; Bottoni, A.; Miscione, G. P. *Organometallics* **2003**, *22*, 940−947. (b) Adlhart, C.; Chen, P. *J. Am. Chem. Soc.* **2004**, *126*, 3496−3510. (c) Costabile, C.; Cavallo, L. *J. Am. Chem. Soc.* **2004**, *126*, 9592−9600.

Scheme 3. Chiral Model Ru-Catalyzed Cyclopropanation Reaction

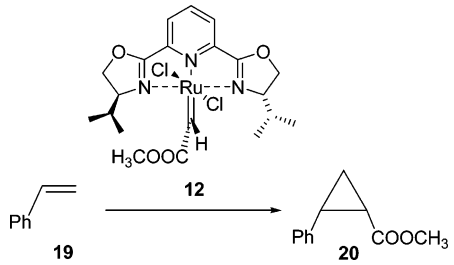

The B3LYP hybrid functional[18] was used throughout the work because of its satisfactory performance in describing the chemistry of transition metals.[19] This functional had already been successfully used in calculations for other ruthenium complexes.[17a] Several different basis sets were used for the calculations, for the sake of comparison. The first one was a hybrid basis set consisting of the Stuttgart−Dresden effective core potential (ECP)[20] for ruthenium and chlorine atoms and the standard 6-31G(d) basis set for the remaining atoms (henceforth SD6-31G*). Geometry optimizations and frequency calculations were carried out with this basis set. Unless otherwise stated, we will only discuss the results obtained at this theoretical level. Some single-point energy calculations were carried out with a hybrid basis set, in which 6-31G(d) was replaced by the 6-311+G(2d,p) basis set (henceforth SD6-311+G(2d,p)). Finally, the LANL2DZ ECP-based basis set[21] was also used for geometry optimizations and frequency calculations. All calculations were carried out using the Gaussian 03 package.[22]

Analytical frequencies were calculated at the same optimization level in all cases, and the natures of the stationary points were determined in each case according to the right number of imaginary frequencies. Scaled frequencies were not considered, since significant errors on the calculated thermodynamic properties are not found at this theoretical level.[23] Solvent effects were taken into account through the IEF-PCM method,[24] as implemented in Gaussian 03. The internally stored parameters of dichloromethane were used to calculate solvation energies.

The key stereoselectivity-determining step was studied using the "real world" model shown in Scheme 3.

Geometrical optimizations and frequency calculations on this model were carried out at the B3LYP/LANL2DZ theoretical level.

(18) (a) Lee, C.; Yang, W.; Parr, R. *Phys. Rev. B* **1988**, *37*, 785−789. (b) Becke, A. D. *J. Chem. Phys.* **1993**, *98*, 5648−5652.
(19) Niu, S.; Hall, M. B. *Chem. Rev.* **2000**, *100*, 353−406.
(20) Fuentealba, P.; Preuss, H.; Stoll, H.; v. Szentpaly, L. *Chem. Phys. Lett.* **1989**, *89*, 418−422.
(21) (a) Hay, P. J.; Wadt, W. R. *J. Chem. Phys.* **1985**, *82*, 270−283. (b) Hay, P. J.; Wadt, W. R. *J. Chem. Phys.* **1985**, *82*, 284−298. (c) Hay, P. J.; Wadt, W. R. *J. Chem. Phys.* **1985**, *82*, 299−310.
(22) Frisch, M. J.; Trucks, G. W.; Schlegel, H. B.; Scuseria, G. E.; Robb, M. A.; Cheeseman, J. R.; Montgomery, Jr., J. A.; Vreven, T.; Kudin, K. N.; Burant, J. C.; Millam, J. M.; Iyengar, S. S.; Tomasi, J.; Barone, V.; Mennucci, B.; Cossi, M.; Scalmani, G.; Rega, N.; Petersson, G. A.; Nakatsuji, H.; Hada, M.; Ehara, M.; Toyota, K.; Fukuda, R.; Hasegawa, J.; Ishida, M.; Nakajima, T.; Honda, Y.; Kitao, O.; Nakai, H.; Klene, M.; Li, X.; Knox, J. E.; Hratchian, H. P.; Cross, J. B.; Bakken, V.; Adamo, C.; Jaramillo, J.; Gomperts, R.; Stratmann, R. E.; Yazyev, O.; Austin, A. J.; Cammi, R.; Pomelli, C.; Ochterski, J. W.; Ayala, P. Y.; Morokuma, K.; Voth, G. A.; Salvador, P.; Dannenberg, J. J.; Zakrzewski, V. G.; Dapprich, S.; Daniels, A. D.; Strain, M. C.; Farkas, O.; Malick, D. K.; Rabuck, A. D.; Raghavachari, K.; Foresman, J. B.; Ortiz, J. V.; Cui, Q.; Baboul, A. G.; Clifford, S.; Cioslowski, J.; Stefanov, B. B.; Liu, G.; Liashenko, A.; Piskorz, P.; Komaromi, I.; Martin, R. L.; Fox, D. J.; Keith, T.; Al-Laham, M. A.; Peng, C. Y.; Nanayakkara, A.; Challacombe, M.; Gill, P. M. W.; Johnson, B.; Chen, W.; Wong, M. W.; Gonzalez, C.; Pople, J. A. *Gaussian 03*, Revision B.04; Gaussian, Inc., Wallingford, CT, 2004.
(23) Bauschlicher, C. W., Jr. *Chem. Phys. Lett.* **1995**, *246*, 40−44.
(24) (a) Tomasi, J.; Mennucci, B.; Cancès, E. *J. Mol. Struct. (THEOCHEM)* **1999**, *464*, 211−226. (b) Cossi, M.; Scalmani, G.; Rega, N.; Barone, V. *J. Chem. Phys.* **2002**, *117*, 43−54 and references therein.

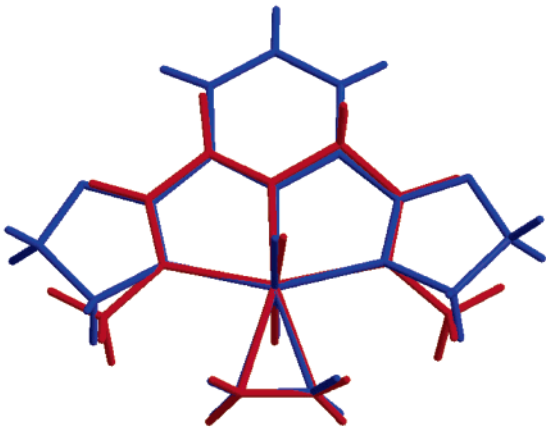

Figure 1. Overlay of the B3LYP/SD6-31G* (red) and the X-ray (blue) geometries of analogous nonchiral complexes.

Hard data on electronic energies, as well as entropies, enthalpies, Gibbs free energies, and lowest frequencies of the different conformations of all structures considered are available as Supporting Information.

Results and Discussion

Catalytic Cycle for the Nonchiral Model. As already indicated in Models and Computational Details, our first concern was to assess whether the nonchiral model proposed is a good representation of the pybox−ruthenium system. With this aim in mind, we calculated the triimine−$RuCl_2$−ethylene complex (**5**) and compared the calculated geometries with the X-ray geometry of an analogous nonchiral pybox−$RuCl_2$−ethylene complex.[25] The RMS-minimized overlay of the B3LYP/SD6-31G(d) and X-ray geometries is shown in Figure 1.

As can be seen, the geometries are almost perfectly superimposed, which indicates that the nonchiral triimine, despite its C_1 symmetry, is a good simple model for the pybox ligand. A more detailed structure of the catalyst−olefin complex **5** is shown in Figure 3. The structure of **5** presents an octahedral coordination for ruthenium, with nonequivalent N(1)−Ru and N(3)−Ru distances. It must be noted, however, that this circumstance also holds in the case of the experimental pybox−$RuCl_2$−ethylene complex structure, although the difference in bond length is slightly smaller (0.02 Å for the experimental structure vs 0.04 Å for the model). Therefore, the lack of C_2 symmetry in the triimine ligand does not seem to cause a significant bias in the geometries of the complexes, and this is an additional indication of that the triimine can be confidently used as a model for the pybox ligand. An energy diagram for the calculated catalytic cycle is displayed in Figure 2. The relative free energies of the structures shown in the diagram (in kcal mol^{-1}) take into account the evolution of the system composition according to the different molecules entering or leaving the system. The catalyst (**6**), ethylene (**1**), methyl diazoacetate (**2**), and dinitrogen (**3**) were arbitrarily chosen as reference points for the calculation of relative free energies. As a consequence of the choice of this reference framework, the catalyst−ethylene complex shown on the right of the diagram is more stable

(25) Nishiyama, H.; Itoh, Y.; Sugawara, Y.; Matsumoto, H.; Aoki, K.; Itoh, K. *Bull. Chem. Soc. Jpn.* **1995**, *68*, 1247−1262.

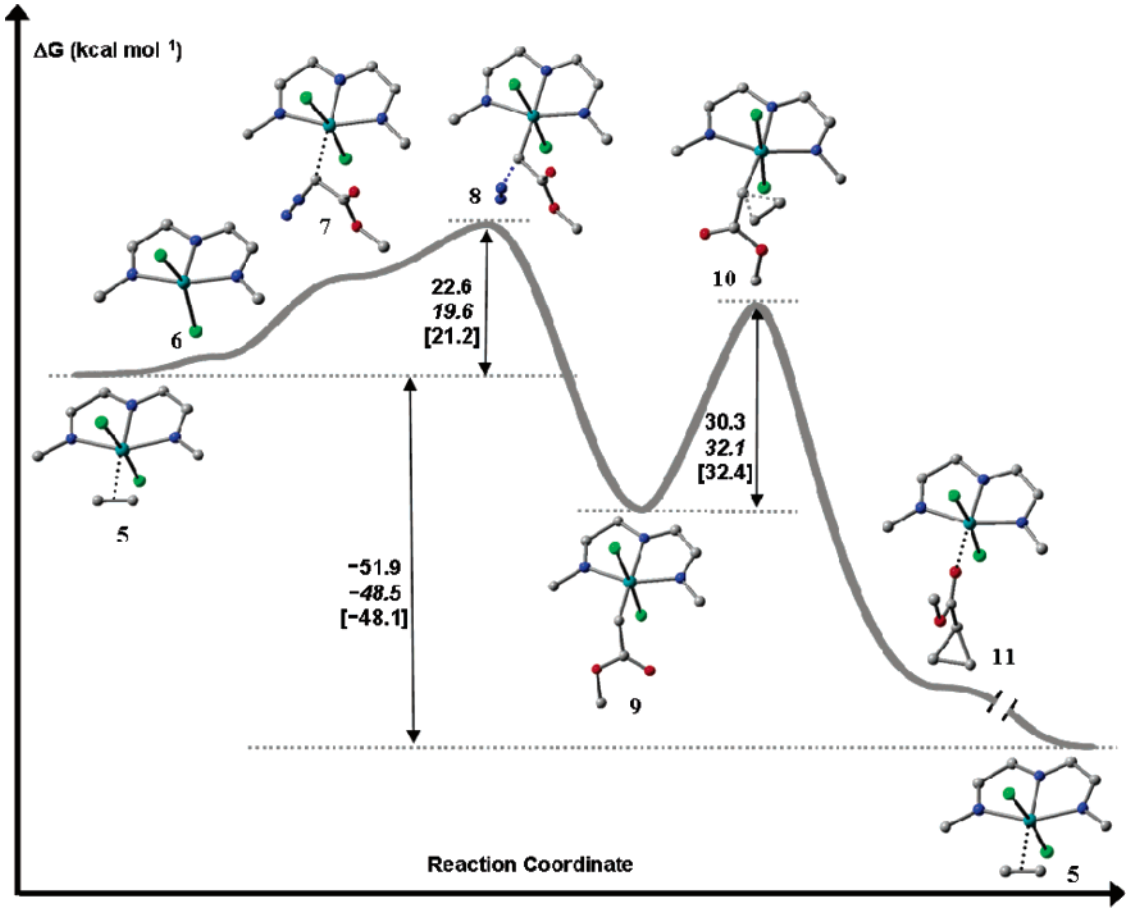

Figure 2. Diagram of B3LYP/SD6-31G(d) (in Roman text), B3LYP/SD6-311+G(2d,p)//B3LYP/SD6-31G* (in italics) and PCM/B3LYP/SD6-31G*//B3LYP/SD6-31G* (in brackets) calculated free energies for a catalytic cycle.

than that situated on the left, since the free energy of the overall cyclopropanation reaction is implicitly included there. The sign criterion of the relative free energy corresponds to the variation in the direction from left to right (according to the diagram).

As can be seen, the catalytic cycle consists of two clear steps. The first step involves the formation of the ruthenium carbene complex, and the second step is the carbene addition to the double bond of the olefin, which occurs in a concerted way. We will comment on both steps in some detail and also describe the intermediates and transition structures (TS) involved in the reaction mechanism.

The formation of the ruthenium carbene intermediate (**9**) must logically proceed through nitrogen extrusion from a previously formed diazo complex (**7**), which in turn comes from the initial catalytic complex **5**. The theoretical calculations indicate that intermediate **7** is formed from **5** by a dissociative ligand exchange mechanism via an intermediate (**6**) that has a coordinative vacancy, in a way similar to that described for a diimine−CuCl complex used to model a bis(oxazoline)−copper catalyst.[26] Transition structures connecting the energy minima corresponding to **5**−**7** could not be located at the theoretical levels used, which indicates that the ligand exchange process is barrierless or, alternatively, has very low activation barriers.

The geometrical parameters shown in Figure 3 illustrate the coordination changes of the ruthenium center. The Ru−ethylene interaction mainly consists of donation of the ethylene π electrons to the Ru center type, as indicated by the C=C length, which is closer to that of free ethylene. The N−Ru distances account for the coordination changes around the ruthenium center. Thus, the N(2)−Ru distance is shorter when there is no ligand in the position trans to N(2) (intermediate **6**). This distance is longer for intermediate **5** than for intermediate **7**, a fact that could be related to the greater coordinating ability of ethylene compared with methyl diazoacetate. Similar behavior can be observed with the N(1)−Ru and N(3)−Ru distances.

Intermediate **7** can extrude a N_2 molecule through TS **8** to give the key ruthenium carbene intermediate **9**. Again, the geometrical changes follow the same systematic trend and the N(2)−Ru distance for the ruthenium carbene intermediate **9** is the longest observed in the whole reaction pathway, indicating strong coordination of the carbene moiety to the ruthenium atom. The sp^2 carbene carbon adopts a perpendicular disposition with regard to the triimine−Ru plane, in agreement with that experimentally observed in the X-ray structure of pybox−$RuCl_2$−carbene complexes.[27] This disposition allows efficient back-donation from one of the d orbitals of Ru to the empty p orbital of the carbene carbon, as visualized in the HOMO plot shown in Figure 4 and corroborated by NBO calculations. The electrophilic character of the carbene carbon also results in an almost perpendicular disposition of the ester group with regard

(26) Fraile, J. M.; García, J. I.; Gil, M. J.; Martínez-Merino, V.; Mayoral, J. A.; Salvatella, L. *Chem. Eur. J.* **2004**, *10*, 758−765.

(27) Nishiyama, H.; Aoki, K.; Itoh, H.; Iwamura, T.; Sakata, N.; Kurihara, O.; Motoyama, Y. *Chem. Lett.* **1996**, 1071−1072.

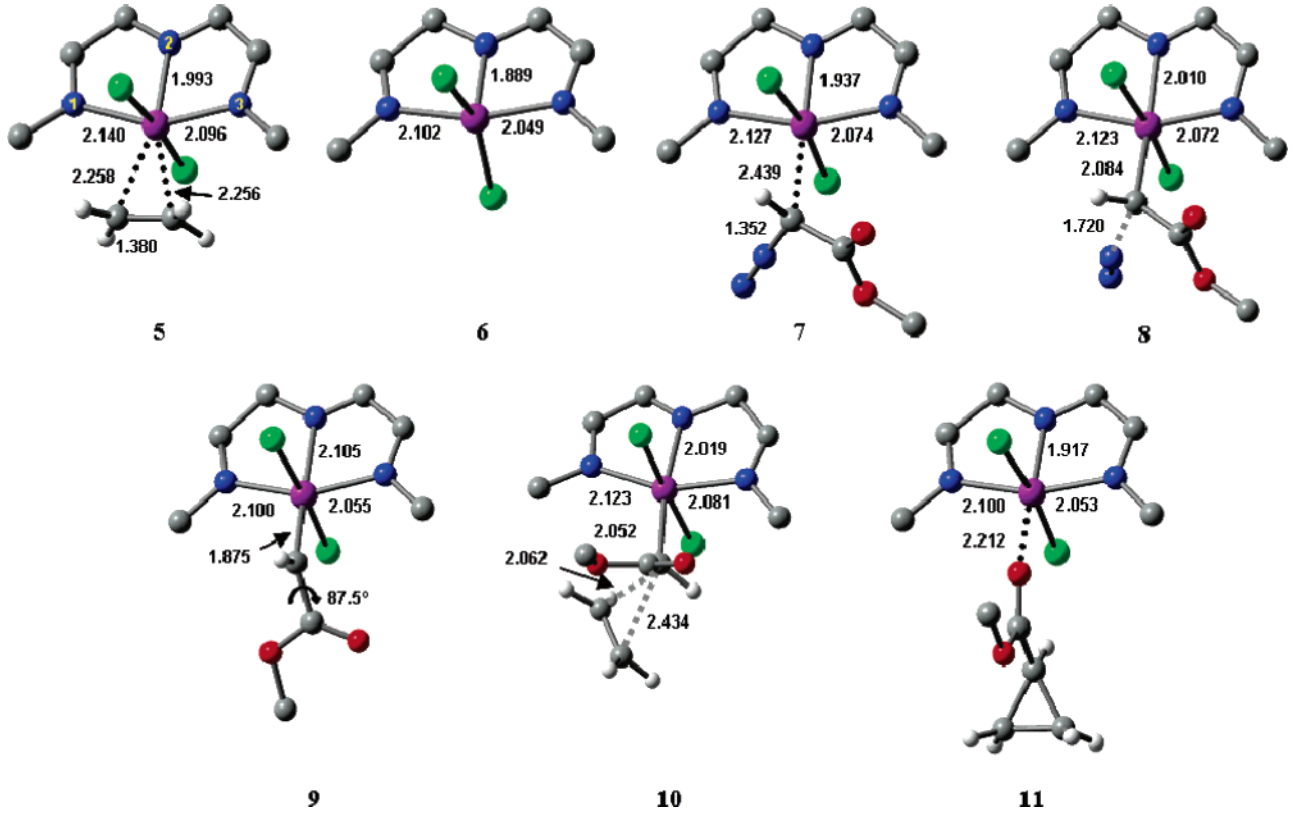

Figure 3. B3LYP/SD6-31G(d) calculated geometries of the reaction intermediates and transition structures in the catalytic cycle. Most of the hydrogen atoms have been omitted for clarity.

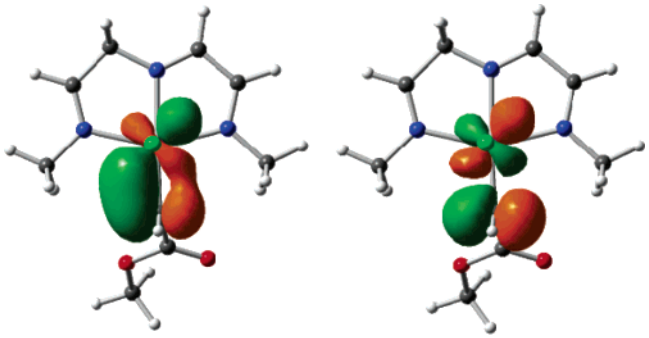

Figure 4. B3LYP/LANL2DZ calculated HOMO and effective LUMO of ruthenium carbene intermediate **9**.

to the $C_{carbene}$−Ru bond, a situation similar to that observed in the case of the copper carbene complexes.[15a,b,26] The effective (for the cyclopropanation reaction) LUMO of the complex largely corresponds to the empty p orbital of the carbene carbon, with the lobes located in the plane of the complex (LUMO + 3 shown in Figure 4). The calculated Gibbs free energy of activation from the initial ethylene complex **5** to form the ruthenium carbene intermediate **9** is 22.6 kcal mol^{-1}, which is also similar to that calculated for the copper-catalyzed cyclopropanation at the B3LYP/6-31G(d) level.[15a,26]

The ruthenium carbene intermediate **9** can react with an ethylene molecule through TS **10** to give the cyclopropane product in a single step. The possibility of a two-step mechanism, via a ruthenacyclobutane, was thoroughly explored, but neither an intermediate complex, with the ethylene coordinated to the ruthenium atom, nor a four-center TS, similar to that described in the case of copper,[15a] could be located. This result contrasts with the situation recently described for a model of Grubbs' complexes,[17a] for which the formation of cyclopropane by a reductive elimination from a ruthenacyclobutane has been described. It is important to note, however, that that model corresponds to a five-coordinate trigonal-bipyramidal ruthenium complex, whereas our model corresponds to a six-coordinate octahedral ruthenium complex, for which the formation of a ruthenacyclobutane intermediate must be much more difficult. TS **10** corresponds to a concerted yet moderately asynchronous reaction pathway, with different C−C bond forming distances (Δd = 0.372 Å) being consistent with the reaction of an electrophilic carbene with an electron-rich olefin bearing a good cation-stabilizing substituent.[8b,15b] The strong interaction between the carbene carbon and the double bond results in a weakening of the Ru−$C_{carbene}$ bond, as indicated by its increase in length from 1.875 Å (**9**) to 2.052 Å (TS **10**), with the concomitant variation in the N(2)−Ru distances due to a trans ligand effect.

The calculated Gibbs free energy of activation for the carbene addition is 30.4 kcal mol^{-1}, which indicates that this is the rate-determining step. This result is in agreement with the higher relative stability observed for ruthenium carbenes with respect to copper or rhodium carbenes.

After the addition step, a complex (**11**) is formed, in which the carbonyl oxygen atom of the cyclopropane product is coordinated to the Ru center. The initial complex **5** must be regenerated from this intermediate in order to close the catalytic cycle. This regeneration

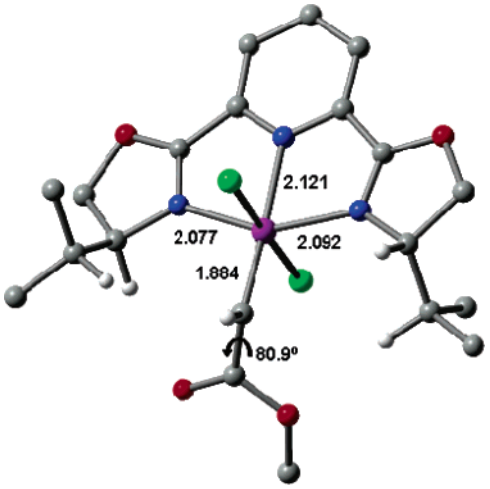

12

Figure 5. B3LYP/LANL2DZ calculated geometry of the lowest energy (^{i}Pr)pybox–$RuCl_2$–carbene complex. Most of the hydrogen atoms have been omitted for clarity.

is energetically favored and is easily accomplished by a dissociative ligand exchange mechanism (not shown in Figure 3).

Free energy results indicate that the overall process is irreversible and largely favored from a thermodynamic viewpoint (−59.1 kcal mol^{-1}).

To test the possible dependence of the results on the basis set used, some calculations on selected structures were carried out with the hybrid SD6-311+G(2d,p), as well as with the LANL2DZ basis sets. Neither the geometries (in the case of LANL2DZ) nor the energies calculated with these basis sets present significant qualitative differences with regard to the SD6-31G* set. Some comparative energy results are shown in Figure 2. The inclusion of solvent effects through PCM calculations (dichloromethane) does not introduce significant changes either. The most noticeable difference found when considering larger basis sets and solvent effects lies in the greater difference in barrier between the first and the second reaction steps (12.5 and 10.2 kcal mol^{-1}, respectively, to be compared with the 7.5 kcal mol^{-1} calculated at the B3LYP/6-31G(d) level), which confirms the second step as being rate determining.

Insights into the Origin of the Stereoselectivity from a "Real World" Chiral Model. First, we calculated the structure of the key (^{i}Pr)pybox–$RuCl_2$–carbene intermediate. Two possible conformations were located—depending on the rotation of the ester group—and both were very close in energy (ΔE = 0.5 kcal mol^{-1}, ΔG = 0.0 kcal mol^{-1}). The B3LYP/LANL2DZ calculated structure of the most stable ruthenium carbene intermediate (**12**) is shown in Figure 5.

As can be seen, most of the relevant geometrical features are very similar to those found for the nonchiral model ruthenium carbene **9**. The carbene carbon adopts a disposition that is perpendicular with regard to the pybox–ruthenium plane. The ester group, in turn, is almost perpendicular to the carbene carbon. As far as the chiral ligand is concerned, it is important to note that the chiral pocket formed by the isopropyl groups around the carbene carbon must result in strong geometrical restrictions for the approach of the reacting alkene molecule. In this regard, it is illustrative to

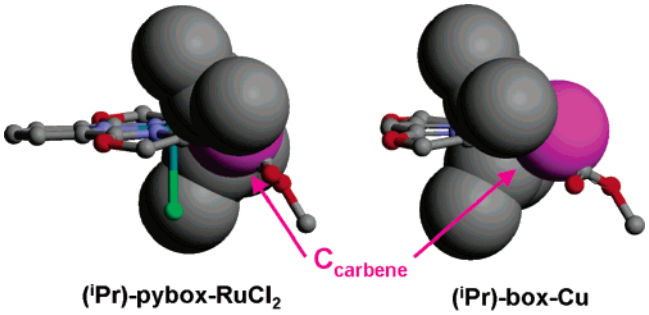

Figure 6. B3LYP/LANL2DZ and B3LYP/6-31G(d) calculated geometries of the (^{i}Pr)pybox–$RuCl_2$–carbene (left) and (^{i}Pr)box–Cu–carbene (right) complexes, respectively. Hydrogen atoms have been omitted for clarity. The carbene carbon is given in magenta.

Table 1. B3LYP/LANL2DZ Calculated Relative Energies and Free Energies (at 298 K) of the TS of the Addition of Ruthenium Carbene 12 to Styrene

TS	ΔE (kcal mol^{-1})	ΔG (kcal mol^{-1})
13-*Re*(I)	0.0	0.0
13-*Re*(II)	0.5	0.0
13-*Si*(I)	2.7	1.7
13-*Si*(II)	3.7	3.5
14-*Re*(I)	3.4	2.6
14-*Re*(II)	2.8	2.4
14-*Si*(II)	6.5	5.9

compare the structure of this intermediate with that of the analogous bis(oxazoline) ligand, (^{i}Pr)box–Cu(I)–carbene, calculated at the B3LYP/6-31G(d) level (Figure 6).

The carbene carbon is much more sterically shielded in the case of the ruthenium complex, most probably due to the different "bite angles" of both ligands, as one of the reviewers suggested, and this has significant consequences for the enantioselectivity of the reaction through the restriction of the approaching trajectories for the alkene (see below). It can be speculated that this is one of the reasons why isopropyl substituents are often sufficient to obtain good enantioselectivities with pybox ligands, whereas *tert*-butyl substituents are necessary for the same reactions in the case of bis(oxazoline) ligands.

We proceeded to calculate the possible TS for the addition of the carbene to the double bond of a styrene molecule. From a stereochemical point of view, there are four possible TS and each leads to one of the possible cyclopropane stereoisomers. These TS correspond to the approach of the alkene to the *Re* or *Si* faces of the carbene carbon, with the phenyl substituent in anti (**13**) or syn (**14**) relative dispositions with regard to the ester group. However, the latter group can adopt two different conformations (as already described in the case of the ruthenium carbene intermediate), which are denoted as I and II. This means that there are in fact eight possible TS. Seven of these eight TS could be effectively located,[28] and their relative energies are gathered in Table 1.

The calculated activation free energy barrier is 24.6 kcal mol^{-1} (this is the lowest value, corresponding to the **13-*Re*(I)** TS), which is somewhat lower than that obtained for the nonchiral model but is still consistent with the addition of the carbene to the alkene being both the rate- and stereoselectivity-determining step.

(28) Every attempt to locate **14-*Si*(I)** resulted in a conformational change of the ester group, leading to **14-*Si*(II)**.

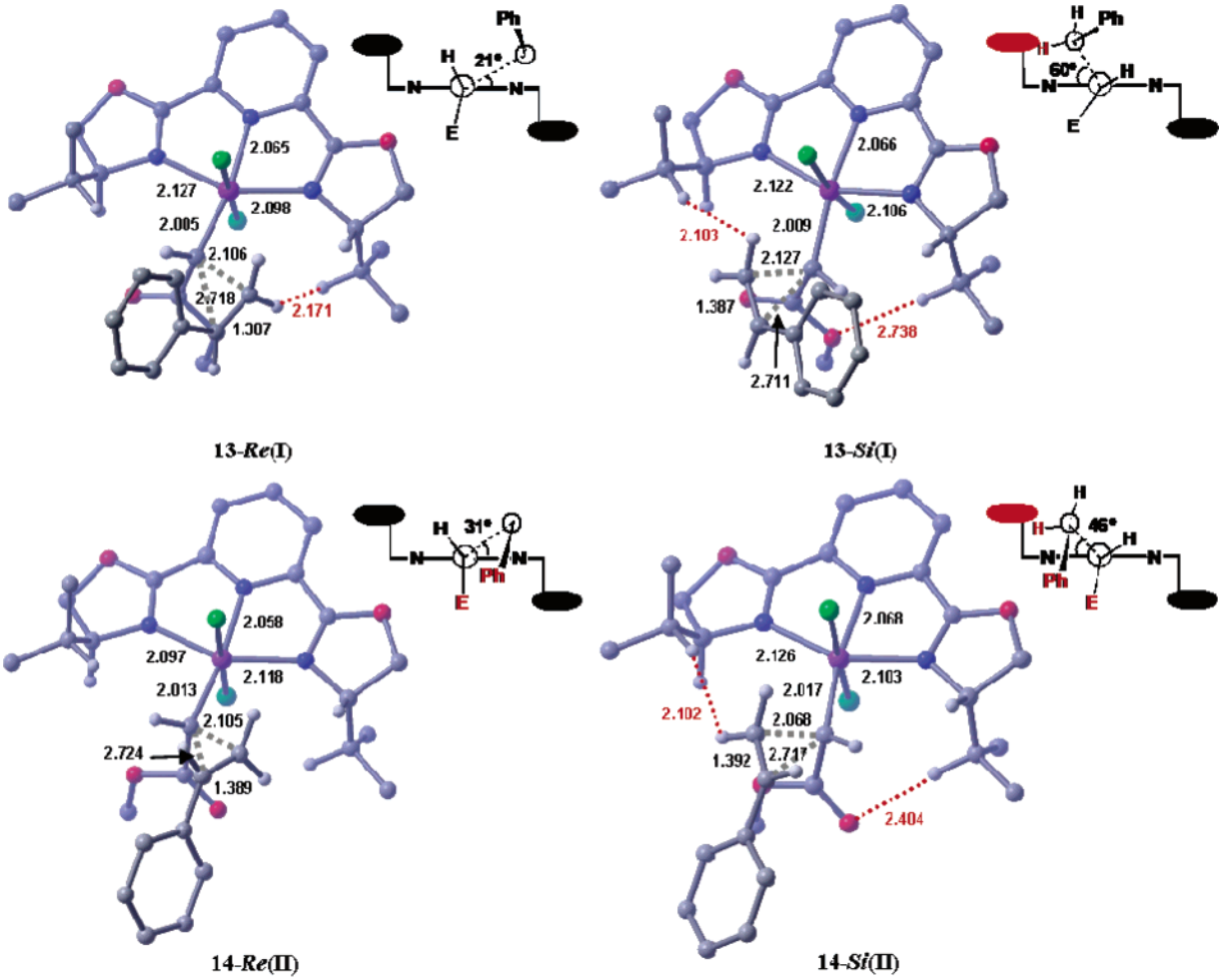

Figure 7. B3LYP/LANL2DZ calculated geometries of the lowest energy transition structures leading to the *trans*- and *cis*-cyclopropanes. The unfavorable steric interactions are shown in red. Most of the hydrogen atoms have been omitted for clarity.

As can be seen from the calculated relative energies (Table 1), the model predicts that the styrene approach preferentially takes place at the *Re* face of the carbene carbon, in both the anti and syn dispositions of the phenyl substituent. This preference leads to the 1*R*,2*R* (*trans*-cyclopropane) and 1*R*,2*S* (*cis*-cyclopropane) major products, respectively—a situation in complete agreement with the experimental results observed for the analogous system with an ethyl ester.[25,29] Of course, it is impossible to be entirely confident about the quantitative predictions, but the large calculated preference for the *Re* approach is qualitatively consistent with the high enantioselectivities obtained with the (^{i}Pr)pybox and other related ligands in cyclopropanation reactions. The model also predicts the clear preference of *trans*- over *cis*-cyclopropanes, again in agreement with the experimental results.

In an effort to gain some insights into the origin of the stereoselectivities observed, we examined the calculated TS structures and compared them with the previously accepted stereodifferentiation models for other analogous catalytic systems. Thus, in the case of bis(oxazoline)−copper catalysts, it has been demonstrated[15a,b] that the origin of the enantioselectivity lies in the steric interaction between the ester group and the substituent in the 4-position of the oxazoline ring in the unfavorable approach of the alkene. This steric interaction is enhanced (in the case of copper catalysts) by the marked axial deviation of the Cu−$C_{carbene}$ bond in the TS.[15a] In other words, the origin of the enantioselectivity for these systems lies in an *intramolecular* steric interaction, which is mediated by the approach of the alkene. On the other hand, the trans/cis selectivity comes from the unfavorable *intermolecular* steric interaction between the ester group of the carbene and the substituent of the alkene (a phenyl group, in the case of styrene).

If we examine the geometries of the lowest energy TS leading to the *trans*-cyclopropanes **13-*Re*(I)** and **13-*Si*(I)** (Figure 7), it can be seen that there do not appear to be any close contacts between the ester group and the isopropyl substituent of the pybox ligand in the "unfavorable" **13-*Si*(I)** TS. The axial deviation of the Ru−$C_{carbene}$ bond is not very significant in any TS (from 8 to 10°). On the other hand, a close contact is observed between one of the C_{β} hydrogen atoms of styrene and the hydrogen atom of the central carbon of the isopropyl group. However, the most prominent difference between the two TS is the dihedral angle C_{β}−$C_{carbene}$−Ru−N, which is 21° in the case of **13-*Re*(I)** and 60° in the case of **13-*Si*(I)** (Figure 7). This dihedral angle can be assimilated to the direction from which styrene ap-

(29) Nishiyama, H.; Itoh, Y.; Matsumoto, H.; Itoh, K. *J. Am. Chem. Soc.* **1994**, *115*, 2223−2224.

proaches the carbene carbon. To minimize the impact of steric effects on this approaching direction, we calculated the corresponding TS in the case where the unsubstituted nonchiral pybox is used.

The calculated $C_\beta-C_{carbene}-Ru-N$ dihedral angle for this TS is 20°, which is very close to that calculated for the favored **13-*Re*(I)** TS. Thus, we propose that, in the absence of noticeable steric interactions, the "preferred" approach angle of styrene in the TS should be close to 20° and that an angle of 60° indicates the presence of a strong steric restriction to this approach. Thus, if we take **13-*Si*(I)** and change the $C_\beta-C_{carbene}-Ru-N$ dihedral angle to 21° by rotation through the $C_{carbene}-Ru$ bond without changing the rest of the geometrical parameters, the resulting distance between the C_β hydrogen atom of styrene and the isopropyl hydrogen atom decreases to 1.365 Å, whereas the distance between the ester oxygen atom and the isopropyl hydrogen atom decreases to 1.662 Å. This operation makes it clear why the approach angle of the styrene must be greater in the case of **13-*Si*(I)**. As the approach angle of styrene changes, the carbene moiety changes in order to maximize the orbital overlap with the alkene.

The consequence of the rotation of the carbene carbon with regard to the pybox−ruthenium complex is the partial loss of Ru−carbene carbon back-donation.

As an indication of the importance of this effect, if the carbene moiety in intermediate **12** is rotated by only 30° from its equilibrium geometry, the resulting energy difference is ca. 1.4 kcal mol^{-1} in the absence of close contacts between the ester and the isopropyl groups. Another geometric feature that enhances the steric interaction between the aforementioned groups is the pyramidalization of the carbene carbon in the TS. This aspect is very similar in all TS but results in the ester and isopropyl groups coming closer to one another in the unfavorable *Si* approaches of styrene.

In conclusion, the stereoelectronic effects derived from a different styrene approach angle seem to be the origin of the higher energy of **13-*Si*(I)** in comparison to **13-*Re*(I)**.

The above hypothesis was further verified by alternately eliminating one or other isopropyl groups from the (^{i}Pr)pybox ligand, an operation that led to the "single-chiral" pybox ligand described by Nishiyama and co-workers.[11] Given the loss of the C_2 symmetry of the ligand, the four possible anti TS become eight. The structures of these eight new TS (labeled as **15** and **16)** were optimized at the B3LYP/LANL2DZ level. A schematic representation of the lowest energy TS leading to the enantiomeric *trans*-cyclopropanes is shown in Figure 8.

As can be seen, there are small changes in geometry and energy in the case of **15-*Re*(I)** and **16-*Re*(I)** with regard to **13-*Re*(I)**, as expected from our hypothesis, given that neither of the isopropyl groups interacts with the incoming styrene. Similarly, **15-*Si*(I)** remains very similar to **13-*Si*(I)**, given that the isopropyl group eliminated is that located on the side opposite to the incoming styrene. However, **16-*Si*(I)**, in which the isopropyl group responsible for the steric repulsion with the incoming styrene is absent, shows clear differences in comparison to **13-*Si*(I)**.

First, the approach angle of styrene decreases, and second, its relative free energy is very close to that of

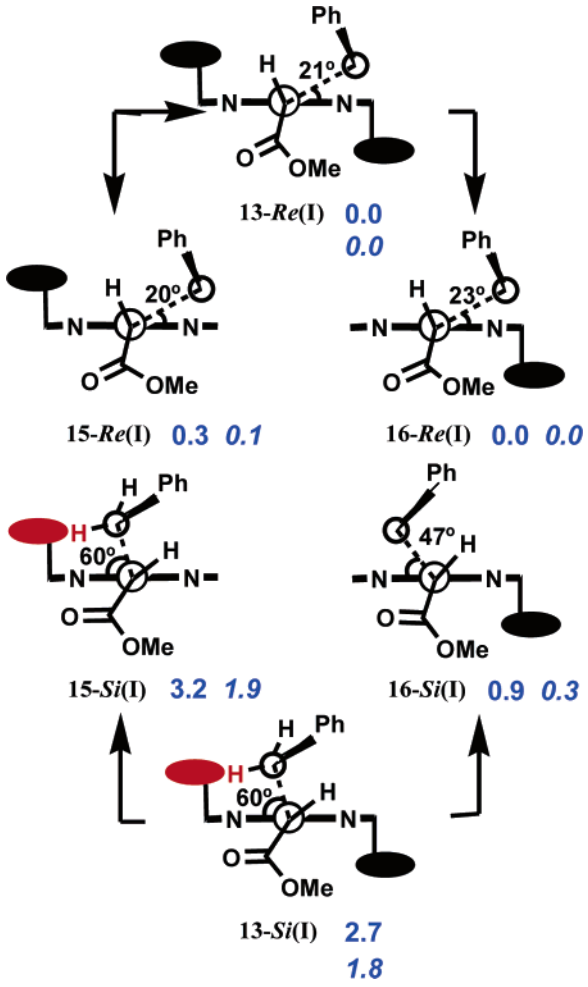

Figure 8. Comparison between the lowest energy anti TS with the (^{i}Pr)pybox ligand and those with a single ^{i}Pr group. The relative energies (plain text) and Gibbs free energies (italics) with regard to the lowest energy TS in each case are shown in blue.

15-*Re*(I) and **16-*Re*(I)**. These results clearly point to the proposed styrene−isopropyl group steric interaction as the main reason for the observed enantioselectivity. These observations also suggest a minor, but relevant, effect of the steric interaction between the ester and isopropyl groups. Thus, **16-*Si*(I)** is somewhat higher in energy than both **15-*Re*(I)** and **16-*Re*(I)**, and the approach angle of styrene is still larger. This situation can be explained by the aforementioned ester−isopropyl group interaction, given that a lower value for the approaching angle would result in a shorter distance between these groups. Once again, a compromise between electronic (orbital overlap) and steric effects must be reached. A similar picture emerges from the examination of the higher energy II conformations of these TS (the structures are given in the Supporting Information). The ester−isopropyl group interaction is even more marked in these conformations, with O···H distances as short as 2.344 Å (**13-*Si*(II)**) and 2.297 Å (**16-*Si*(II)**).

A similar reasoning can be invoked to explain the enantioselectivity in the case of the syn TS, which leads to *cis*-cyclopropanes. Thus, the approach angle of the styrene is 31° in the case of **14-*Re*(II)**, a value very similar to that found in **10**. On the other hand, this angle increases to 46° in the case of **14-*Si*(II)**, which

Table 2. B3LYP/LANL2DZ Calculated Relative Energies and Free Energies (at 298 K) of the TS Bearing an NH_2 Substituent in the Pybox Ligand

TS	ΔE (kcal mol^{-1})	ΔG (kcal mol^{-1})
17-*Re*(I)	0.0	0.0
17-*Si*(I)	1.9	1.2
18-*Re*(II)	2.8	2.0
18-*Si*(II)	6.2	5.0

can be explained by the presence of both styrene−isopropyl group interactions (H···H distance of 2.183 Å) and ester−isopropyl group interactions (O···H distance of 2.404 Å). If the approach angle is reduced to 31°, then these distances further decrease to 1.825 and 2.167 Å, respectively. We can therefore conclude that the main origin of the enantioselectivity lies in the *intermolecular* styrene−ligand steric interaction—a situation that also occurs in the case of the syn TS—whereas the *intramolecular* ester−ligand steric interaction plays a secondary, but still nonnegligible, role. This scenario is consistent with the fact that the best enantioselectivities are obtained with bulky esters, such as menthyl and *tert*-butyl esters; although these systems are only marginally better than those obtained with the diazoacetate ethyl ester (from 88% ee to 94% ee in the *trans*-cyclopropanes, which represent an energy difference of only 0.4 kcal mol^{-1}).[11,29]

Of course, the trans/cis diastereoselectivity is much easier to explain, given that it arises almost exclusively from the styrene−ester steric interaction. In fact, it has been reported that the completely unsubstituted pybox ligand leads to a trans/cis selectivity identical with that found with the chiral (^{i}Pr)pybox ligand.[11]

Testing the Performance of the Model. To test the scope of the model developed, we applied it to two interesting experimental observations that are not particularly easy to explain.

The remote stereoelectronic effect observed when the pyridine ring is 4-substituted was considered first. It has been reported[10] that electron-donating substituents, such as the dimethylamino group, decrease the enantioselectivity in both *trans*- and *cis*-cyclopropanes, whereas the trans/cis selectivity remains unchanged. This effect is quantitatively greater than the almost negligible improvement in enantioselectivity observed with electron-withdrawing groups, and this is the reason for which it was chosen as a testing system. Unfortunately, the experimental results correspond to the reaction of *l*-menthyl diazoacetate rather than methyl or ethyl diazoacetate. Despite this, we calculated the four TS analogues to **13-*Re*(I)**, **13-*Si*(I)**, **14-*Re*(II)**, and **14-*Si*(II)**, but with an amino (NH_2) group in the 4-position of the pyridine ring. The relative energies of these TS are gathered in Table 2.

If we compare the relative free energies obtained for the unsubstituted pybox with those obtained for the NH_2-substituted pybox, it is clear that the energy difference decreases both for the anti and syn TS.

Thus, the free energy difference between **13-*Re*(I)** and **13-*Si*(I)** is 1.7 kcal mol^{-1}, whereas that between **17-*Re*(I)** and **17-*Si*(I)** is 1.2 kcal mol^{-1}. In the case of the syn TS, the free energy difference between **14-*Re*(II)** and **14-*Si*(II)** is 3.5 kcal mol^{-1}, whereas between **18-*Re*(II)** and **18-*Si*(II)** it is 3.0 kcal mol^{-1}. It is clear that these are very small differences (as are the experimental values), and they must be treated with caution. However, the trend is in agreement with the experimental observations.

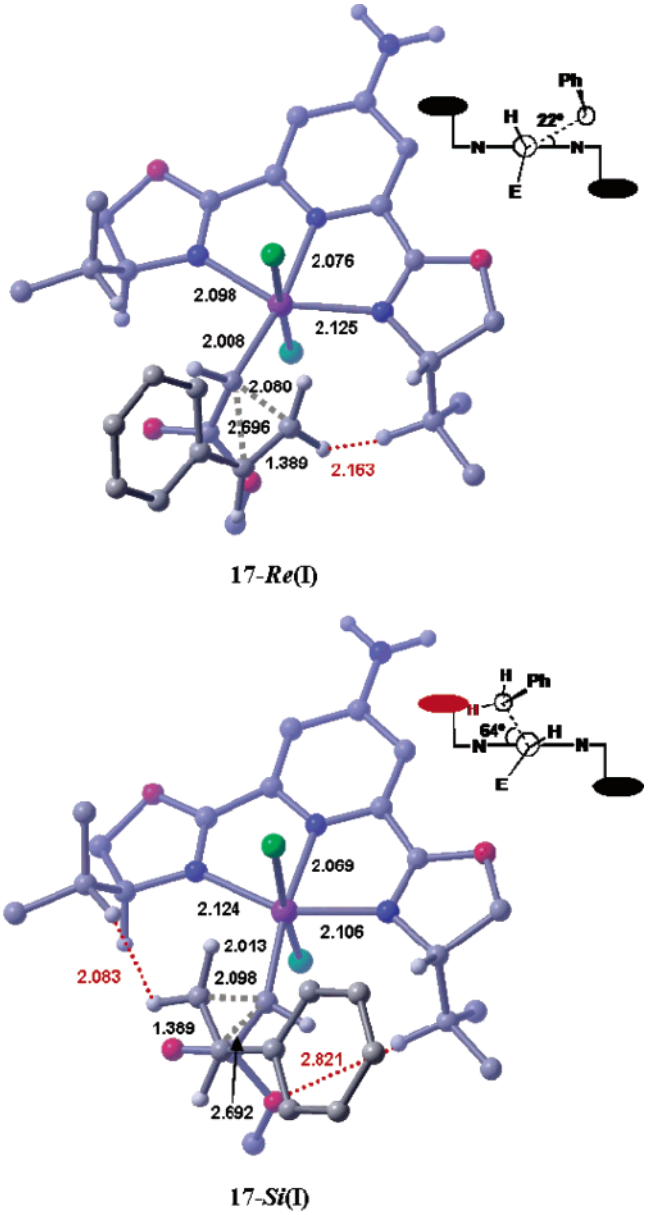

Figure 9. B3LYP/LANL2DZ calculated geometries of the lowest energy transition structures leading to the *trans*-cyclopropanes. The unfavorable steric interactions are shown in red. Most of the hydrogen atoms have been omitted for clarity.

As far as the origin of these differences is concerned, the calculated geometries (Figure 9) indicate that there are very small differences in all of the geometrical parameters, apart from the C−C bond forming distances. In the case of the NH_2-substituted pybox, the four TS are later than their corresponding unsubstituted pybox counterparts, which is undoubtedly due to the electron-donating character of the amino group making the carbene less electrophilic. A number of small differences are also apparent in the synchronicity of the TS, such that **17-*Re*(I)** and **17-*Si*(I)** are closer in synchronicity (Δd = 0.616 and 0.594 Å, respectively) than **13-*Re*(I)** and **13-*Si*(I)** (Δd = 0.612 and 0.584 Å, respectively). This similarity may be related to the closer energies resulting from small variations of the close

contact distances. Similar considerations hold for the corresponding syn TS.

The second interesting effect concerns the good enantioselectivities obtained with the "single chiral" pybox ligand bearing only one isopropyl substituent.[11] It can be clearly seen from the results given in Figure 8 and in the Supporting Information that our model is able to explain this unusual result. For instance, comparison between **15-*Re*(I)**, **15-*Si*(I)**, **16-*Re*(I)**, and **16-*Si*(I)** indicates that a good enantioselectivity in *trans*-cyclopropanes is to be expected on the basis of the same steric interactions responsible for the enantioselectivity observed with the C_2-symmetric ligand. Full details on this system have recently been reported as a short communication,[30] and therefore, this aspect will not be discussed here.

Conclusions

DFT calculations allow us to propose a reaction mechanism for the cyclopropanation reactions of olefins catalyzed by ruthenium−pybox complexes that is fully consistent with experimental data observed for these systems. Under the reaction conditions most of the catalyst is coordinated with one olefin molecule. Thus, the catalyst−ethylene complex is considered as the starting species for a catalytic cycle. Ethylene can be replaced by the diazo ester through a dissociative ligand exchange mechanism. The catalyst−diazo compound can extrude nitrogen to yield a ruthenium carbene complex. This ruthenium carbene is able to react with an olefin molecule through a concerted mechanism that leads to the cyclopropane product. The calculated activation barrier of this step is higher than that of the nitrogen extrusion step, meaning that this is the rate-determining step of the reaction. This situation is consistent with the greater relative stability of the ruthenium carbene complexes in comparison to those of copper or rhodium. The resulting catalyst−cyclopropane complex can easily regenerate the catalyst−ethylene complex through a dissociative ligand exchange. The overall catalytic cycle is highly exergonic (ca. 52 kcal mol^{-1}).

A "real world" system, namely the cyclopropanation reaction of styrene with methyl diazoacetate catalyzed by the dichloro-(2,6-bis[(*S*)-4-isopropyloxazolin-2-yl]pyridine) ruthenium(II) complex, was used to account for the stereoselectivity of the reaction. The results of the DFT calculations are in excellent agreement with the observed enantioselectivities and trans/cis selectivity. Careful examination of the optimized geometries of the TS allowed an enantiodifferentiation mechanism to be proposed on the basis of the intermolecular steric interaction between the incoming styrene molecule and one of the pybox isopropyl groups in the *Si* approach. The intramolecular steric interaction between the ester group and one of the pybox isopropyl groups also plays a secondary, but still significant, role. This enantiodifferentiation mechanism contrasts with that previously reported for the bis(oxazoline)−copper(I) catalysts and clearly illustrates how the subtle geometrical changes in the TS derived from the changes in metal and ligand markedly modify the steric requirements of the reactions. As a corollary, it can be concluded that establishing a priori analogies to explain the behavior of different catalytic systems, even for the same reaction and following the same reaction mechanism, can give rise to misleading conclusions.

The scope of the asymmetric induction model developed has been tested by applying it to two particularly difficult problems, namely (i) the remote stereoelectronic effect of substituents in the 4-position of the pyridine ring and (ii) the high enantioselectivities observed with asymmetric pybox ligands (bearing only one isopropyl group). In both cases, the model has been able to explain these experimental results in a satisfactory way.

In summary, a thorough examination of the potential energy surface of the model reaction studied has allowed the elucidation of the key steps in the mechanism of ruthenium-catalyzed cyclopropanation reactions. This information provides new and valuable insights into the origin of the stereoselectivities observed, which should allow the design of more efficient catalytic systems.

Acknowledgment. This paper is dedicated to Prof. José Elguero on the occasion of his 70th birthday. This work was made possible by the generous financial support of the Comisión Interministerial de Ciencia y Tecnología (Project PPQ2002-04012), the Diputación General de Aragón (Grupo Consolidado Catálisis Heterogénea en Síntesis Orgánicas Selectivas), and the Navarra Government (Res. 5/2003).

Supporting Information Available: Tables of electronic energies, as well as enthalpies, entropies, Gibbs free energies (the last three data series at 25 °C), and the lowest frequencies for the different conformations of the structures considered in this work, and tables giving Cartesian coordinates of the structures discussed in the paper. This material is available free of charge via the Internet at http://pubs.acs.org.

OM050300V

(30) Cornejo, A.; Fraile, J. M.; García, J. I.; Gil, M. J.; Martínez-Merino, V.; Mayoral, J. M.; Salvatella, L. *Angew. Chem., Int. Ed.* **2005**, *44*, 458−461.